Brain Pathology ISSN 1015-6305

RESEARCH ARTICLE

Transient Peripheral Immune Response and Central Nervous System Leaky Compartmentalization in a Viral Model for Multiple Sclerosis

María José Navarrete-Talloni[1,2]; Arno Kalkuhl[3]; Ulrich Deschl[3]; Reiner Ulrich[1,2]; Maren Kummerfeld[1]; Karl Rohn[4]; Wolfgang Baumgärtner[1,2]; Andreas Beineke[1,2]

[1] Departments of Pathology and [4] Biometry, Epidemiology and Information Processing, University of Veterinary Medicine Hanover, Hanover, Germany.

[2] Center for Systems Neuroscience Hanover, Hanover, Germany.

[3] Department of Non-Clinical Drug Safety, Boehringer Ingelheim Pharma GmbH & Co KG, Biberach (Riß), Germany.

Keywords

DNA microarray analysis, deep cervical lymph node, encephalomyelitis, immune responses, multiple sclerosis, SJL-mice, Theiler's murine encephalomyelitis virus.

Corresponding author:

Prof. Dr. Andreas Beineke, Department of Pathology, University of Veterinary Medicine Hanover, Bünteweg 17, D-30559 Hanover, Germany (E-mail: *andreas.beineke@tiho-hannover.de*)

Received 28 October 2009; accepted 2 February 2010.

doi:10.1111/j.1750-3639.2010.00383.x

Abstract

Theiler's virus-induced demyelination represents an important animal model to study the chronic-progressive form of multiple sclerosis (MS). The aim of the present study was to identify specific genes and pathways in the deep cervical lymph node (cLN) and spleen of experimentally infected SJL-mice, using DNA microarrays. Analyses identified 387 genes in the deep cLN and only 6 genes in the spleen of infected animals. The lymph node presented 27.4% of genes with fold changes ± 1.5 at 14 days post infection (dpi) and a reduced transcription at later time points. *K*-means clustering analyses resulted in five clusters. Accordingly, functional annotation revealed that the B-cell immune response pathway was the most up-regulated cluster at the early phase. Additionally, an increase of CD68- and lysozyme-positive cells in the deep cLN was observed by immunohistochemistry. Polioencephalitis was most intense at 14 dpi, and the spinal cord demyelinating leukomyelitis started at 42 dpi.

In summary, early gene expression is indicative of virus-trigged immune responses in the central nervous system (CNS)-draining lymph node. The decreased gene transcription in the deep cLN during the chronic phase and the low number of spleen genes supports the hypothesis of a compartmentalized inflammation within the CNS, as described in progressive MS.

INTRODUCTION

Multiple sclerosis (MS), one of the most frequent central nervous system (CNS) diseases in young adults, is a chronic demyelinating disease of unknown etiology and possibly multifactorial causes. Based on the generation of myelin-specific immune responses, MS is regarded as an autoimmune disease (6, 65); however, virus infections (21, 38, 67), environmental factors (39) and genetic disorders (10, 11) are discussed as initiating events or predispositions, respectively. Further investigations demonstrated that disease progression in MS is associated with the development of a compartmentalized immune response, including intrathecal antibody production trapped behind a closed blood brain barrier (BBB) (43, 75). A variety of MS subtypes has been defined based on the clinical progression of the disease (9, 76, 80). To study the chronic-progressive form of MS, the Theiler's murine encephalomyelitis (TME) is commonly used as a viral animal model (14, 58, 62, 86). Intracerebral infection with the low virulent BeAn-strain of the Theiler's murine encephalomyelitis virus (TMEV), a picornavirus, causes an acute virus-induced polioencephalitis in mice (48), characterized by an infiltration of virus-specific $CD4^+$ and $CD8^+$ T-cells, as well as B-cells and macrophages in the brain (23, 64). While resistant C57/BL6-mice eliminate the virus from the cerebral gray matter after the acute phase by specific cellular immunity (62), inadequate viral clearance in SJL-mice leads to viral persistence predominately in macrophages and/or glial cells (30, 82). Subsequently, delayed type hypersensitivity and myelin-specific autoimmunity are supposed to induce demyelination in the spinal cord white matter during the chronic phase (48, 61, 81, 82).

The majority of the animal models for MS, including experimental autoimmune encephalomyelitis (EAE) and TME, have focused upon the characterization of immune responses within the CNS. So far, most investigations of the peripheral immune regulation have been performed in EAE models, while only few studies investigated the involvement of lymphoid organs in TMEV-infected mice (54, 56, 63) despite their importance in the pathogenesis of demyelinating diseases (47). Although classical lymphatic vessels are lacking in the CNS, the cerebrospinal fluid and

interstitial fluid drain to the regional lymph nodes (1, 12). Brain-derived antigens are transported mostly to the cervical lymph nodes [cLNs; (8, 89, 91)]. Further, it has been demonstrated in rodents that the spinal cord drains primarily to the cLNs and to the lumbar lymph nodes (34, 89). CNS-derived myelin has been detected in cLN of MS patients (20, 92) and in a marmoset model of EAE (16), suggesting that these lymphoid organs represent the anatomical sites of antigen presentation and activation of encephalitogenic immune cells. Accordingly, studies have shown that the cLN represent the organs where T-cells targeting the brain are primed during the initiation of EAE in the rat brain (40, 69). Similarly, Van Zwam *et al* (87) reported the significance of CNS-draining lymph nodes for epitope spreading and priming of myelin-specific immune responses in murine EAE. In autoimmune CNS disorders, the cLNs are supposed to host dendritic cells (DC) from the brain, which initiate and propagate a CNS-directed response, as demonstrated in EAE in rats (28). Furthermore, chemokine-mediated accumulations of DC in brain-draining lymph nodes have been detected during the priming and effector phase of EAE in mice (50). However, investigations upon the role of lymph nodes in MS animal models show contradictory and conflicting results. Referring to this, McMahon *et al* (54) demonstrated that epitope spreading and T-cell activation is restricted to the CNS in TMEV and EAE. In addition, myelin-specific lymphocytes can be activated within the CNS without previous priming in peripheral lymphoid organs, as observed in a murine EAE model (24).

The cLNs are crucial organs for the initiation and control of immune responses following CNS infection of neurotropic viruses, including rubella virus, varicella-zoster virus, herpes simplex virus, Epstein-Barr virus and human immunodeficiency virus (88, 91). Further, picornaviruses, such as TMEV and Coxsackie virus, are able to stimulate virus-specific immune responses in brain-draining lymph nodes (63). In TMEV, a virus-specific T-cell response is activated in the cLN followed by migration to and expansion within the brain (56).

DNA microarray analyses have been used to determine gene expression in human MS and its animal models (2, 26, 32, 59, 60). Recently, genes and pathways associated with intrathecal antibody production, antigen processing, and presentation have been detected in the spinal cord of TMEV-infected mice, supporting the view of an intact BBB and local immune responses within the CNS during disease progression (85). Therefore, the aim of the present study was to identify transcriptional changes in the CNS-draining cLN and spleen associated with disease initiation and to test the hypothesis of a CNS compartmentalization of the immune response during demyelination in this murine MS model.

MATERIALS AND METHODS

Experimental design

Forty-eight 5-week-old female SJL/J HanHsd mice (Harlan Winkelmann, Borchen, Germany) were inoculated into the right cerebral hemisphere with 1.63×10^6 plaque-forming units/mouse of the BeAn-strain of TMEV in 20 µL Dulbecco's Modified Eagle Medium (PAA Laboratories, Cölbe, Germany) with 2% fetal calf serum and 50 µg/kg gentamycin. Sham-infected animals received 20 µL of the vehicle only. Inoculation was carried under general anesthesia with medetomidine (0.5 mg/kg, Domitor®, Pfizer, Karlsruhe, Germany) and ketamine (100 mg/kg, ketamine 10%, WDT eG, Garbsen, Germany). All experiments were performed in groups of six TMEV- and sham-infected mice, euthanized 1 h after intracerebral inoculation [0 days post infection (dpi)], as well as 4, 7, 14, 42, 98 and 196 dpi, except for five TMEV-infected mice at 98 dpi. For histology, immunohistochemistry and *in situ* hybridization, brain, deep cLN (*Ln. cervicalis profundus cranialis*), and spleen were removed immediately after death and fixed in 10% formalin for 24 h and embedded in paraffin wax. In addition, spinal cord segments encased within the first cervical vertebral body, third and fourth thoracic vertebral bodies, and the first lumbar vertebral body of the spinal column were formalin fixed, decalcified in 10% ethylenediaminetetraacetic acid solution for 48 h, and subsequently embedded in paraffin wax (84).

For microarray analysis, the deep cLN and spleen were immediately removed, snap-frozen in liquid nitrogen and stored at −80°C. The animal experiments were authorized by the local authorities (Niedersächsisches Landesamt für Verbraucherschutz- und Lebensmittelsicherheit, Oldenburg, Germany, permission number: 33-42502-05/963).

Brain and spinal cord histological examination

Transversal sections of formalin-fixed, paraffin-embedded cerebrum, cerebellum, brainstem and spinal cord segments were stained with hematoxylin and eosin (HE). Inflammatory responses within the CNS were graded based upon the degree of perivascular infiltrates (PVI) using a semiquantitative scoring system: 0 = no changes, 1 = scattered perivascular infiltrates, 2 = two to three layers of perivascular inflammatory cells, 3 = more than three layers of perivascular inflammatory cells, as described previously (23). For the evaluation of myelin loss, serial sections of spinal cord were stained with Luxol fast blue-cresyl violet (LFB-CV) and the degree of demyelination was semi-quantitatively evaluated as follows: 0 = no change, 1 = 25%, 2 = 25–50% and 3 = 50–100% of the white matter affected (23).

Employing the Mann-Whitney U-test, statistical comparisons between TMEV-infected and sham-infected mice were assessed, and one-way ANOVA with Tukey *post-hoc* test was performed to calculate statistical differences among 14, 42, 98, and 196 dpi for the semiquantitative scores obtained in the brain and the spinal cord. Analyses were performed using SPSS for Windows (Version 14.0, SPSS Inc., Chicago, IL). A *P-value* of less than 0.05 was considered as statistically significant.

RNA isolation and microarray hybridization

Microarray analyses of the deep cLN and spleen were performed at 14, 42, 98 and 196 dpi. RNA from lymphoid organs was isolated from quick frozen tissues using TRIzol® reagent (Invitrogen, Karlsruhe, Germany) followed by isolation using the RNeasy® Mini Kit (Qiagen, Hilden, Germany), including DNAse digestion, according to the manufacturer's protocol. RNA quality was assessed in an Agilent 2100 Bioanalyzer (Agilent Technologies, Böblingen, Germany) using the Agilent RNA 6000 Nano Kit. From each sample, 250 ng of total RNA was amplified and labeled with the MessageAmp™ II-Biotin Enhanced Kit (Ambion, Austin, TX). Hybridization of the cRNA to GeneChip® mouse genome 430 2.0 arrays (Affymetrix, Santa Clara, CA) and following steps were

processed as described before (85). Minimum information about a microarray experiment compliant data sets will be published following acceptance in the ArrayExpress database (http://www.ebi.ac.uk/microarray-as/ae/).

Detection of differentially expressed genes

Primary microarray data were analyzed with the genechip operating software (GCOS, Affymetrix), followed by background adjustment and quantile normalization computed via robust multichip average (7), using the RMAExpress package from PartekPro™ (Partek Inc., St. Louis, MO). Data homogeneity was verified using principal components analysis (Partek® Genomics Suite™ 6.2, St. Louis, MO). Statistical analysis was done using $\log_2$ transformed expression data. Gene expression among all time points was investigated employing a natural cubic spline-based method insert in extraction of differential gene expression (EDGE) (45, 78). A *Q*-value of <0.05, which represents a false discovery rate (FDR) of 5.0%, was selected as cutoff to determine significant differences in gene expression. Differentially expressed genes were grouped by *k*-means clustering (77) of the $\log_2$ mean fold changes (FCs) for each individual time point, using Euclidean distance to create consensus clusters, visualized through heat maps (MeV v4.3.01, insert in TM4 suite) (74).

For all the resulting gene probe sets, ontology information was assigned employing the database for annotation, visualization and integrated discovery (DAVID) (17, 31). When several probe sets matched a single gene symbol, the probe set with a lower *Q*-value and higher FC was selected for the analyses. Significantly enriched pathways were selected from the biological process category of the gene ontology database at a FDR of 1.0% (3).

Virus detection

Virus dissemination during the early (0, 4, 7 and 14 dpi) and late time points (42, 98 and 196 dpi) was investigated by immunohistochemistry and *in situ* hybridization in the brain, spinal cord, deep cLN, and spleen.

Immunohistochemistry was performed using a polyclonal rabbit anti-TMEV capsid protein VP1-specific antibody, as described before (36). Briefly, for blocking of the endogenous peroxidase, formalin-fixed, paraffin-embedded tissue sections were treated with 0.5% H_2O_2 diluted in methanol for 30 minutes at room temperature (RT). Subsequently, slides were incubated with the primary antibody at a dilution of 1:2000 for 16 h at 4°C. Goat-antirabbit IgG diluted 1:200 (BA9200, H+L, Vector Laboratories, Burlingame, CA) was used as a secondary antibody for 1 h at RT. Sections used as negative controls were incubated with rabbit normal serum at a dilution of 1:2000 (Sigma-Aldrich Chemie GmbH, Taufkirchen, Germany). Slides were subsequently incubated with the peroxidase-conjugated avidin-biotin complex (ABC method, PK-6000, Vector laboratories) for 30 minutes at RT. After the positive antigen-antibody reaction visualization by incubation with 3.3-diaminobenzidine-tetrachloride in 0.1 M imidazole, sections were counterstained with Mayer's hematoxylin.

In situ hybridization was performed as described before (25, 84). For the detection of TMEV-specific RNA, a polymerase chain reaction product homologous to the base pair 193–322 of the nucleotide sequence for BeAn 8386 strain (68) was generated from a TMEV-infected baby hamster kidney cell culture by reverse transcriptase-polymerase chain reaction using the sense primer 5′GACTAATC AGAGGAACGTCAGC and the anti-sense-primer 5′GTGAA GAGCGGCAAGTGAGA. The obtained polymerase chain reaction (PCR) product was cloned in the PCR 4-TOPO plasmid vector and amplified in DH5α-T1® cells (TOPO TA Cloning Kit for sequencing; Invitrogen). The plasmid was sequenced (SEQLAB, Göttingen, Germany) and the sequence is accessible under the GenBank® (accession number: AY618571). *In vitro* transcription was carried out according to the manufacturer's instructions with DIG-RNA-labeling Mix and T3- and T7-RNA-polymerases (Roche Diagnostics, Mannheim, Germany). Tissue sections were dewaxed in xylene, hydrated in graded ethanol and washed in ultrapure, pyrogen-free, diethylpyrocarbonate-treated water (Sigma-Aldrich Chemie; 0.1% in ultrapure, pyrogen-free water). After proteolyses (5 µg/mL, proteinase K; Roche Diagnostics), acetylation and prehybridization, hybridization was performed overnight in a moist chamber at 52°C with a probe concentration of 200 ng/mL. The detection system consisted of an anti-DIG-antibody conjugated with alkaline phosphatase (1:200; Roche Diagnostics) and the substrates nitroblue tetrazoluimchloride (both Sigma-Aldrich Chemie) and 5-bromo-4-chloro-3-indolyl phosphate (X-Phosphate) (Sigma-Aldrich Chemie), which yielded a bluish precipitate. Positive reactions were observed and notated as absolute numbers.

Immunophenotyping of deep cLN

Microarray results of the deep cLN were substantiated by immunohistochemistry using a CD68-specific marker (monoclonal rat anti-mouse, clone FA-11, diluted 1:20; Abcam Ltd, Cambridge, UK) and a lysozyme-specific marker (polyclonal rabbit antihuman, diluted 1:250; Dako Corporation, Carpintería, CA). Briefly, affinity-purified, mouse-adsorbed rabbit antirat IgG diluted 1:200 (BA 4001; Vector Laboratories) and goat-antirabbit IgG diluted 1:200 (BA9200, H+L; Vector Laboratories), respectively, were used as secondary antibodies for 1 h at RT. Sections used as negative controls were incubated with IgG_{2a} at a dilution of 1:100 (clone 54 447; R&D Systems, Minneapolis, MN) or rabbit normal serum at a dilution of 1:2000 (Sigma-Aldrich Chemie GmbH), respectively.

The percentages of CD68- and lysozyme-positive cells in lymph node follicles, subcapsular sinuses, and paracortical zones were determined by counting labeled and unlabeled cells in the respective areas.

A two-way ANOVA with consideration of variance interaction and *post-hoc* test for multiple pairwise comparisons with Bonferroni adjustment was employed for the $\log_{geo}$-transformed immunohistochemistry data. The Statistical Analysis System, version 9.1 (SAS Institute, Cary, NC) was used to determine statistical differences between TMEV-infected and sham-infected SJL-mice. A *P*-value of less than 0.05 was considered as statistically significant.

RESULTS

TMEV-induced demyelinating disease

The highest degree of inflammation within the brain was found at 14 dpi (Figure 1A,B), followed by a decline of the PVI scores

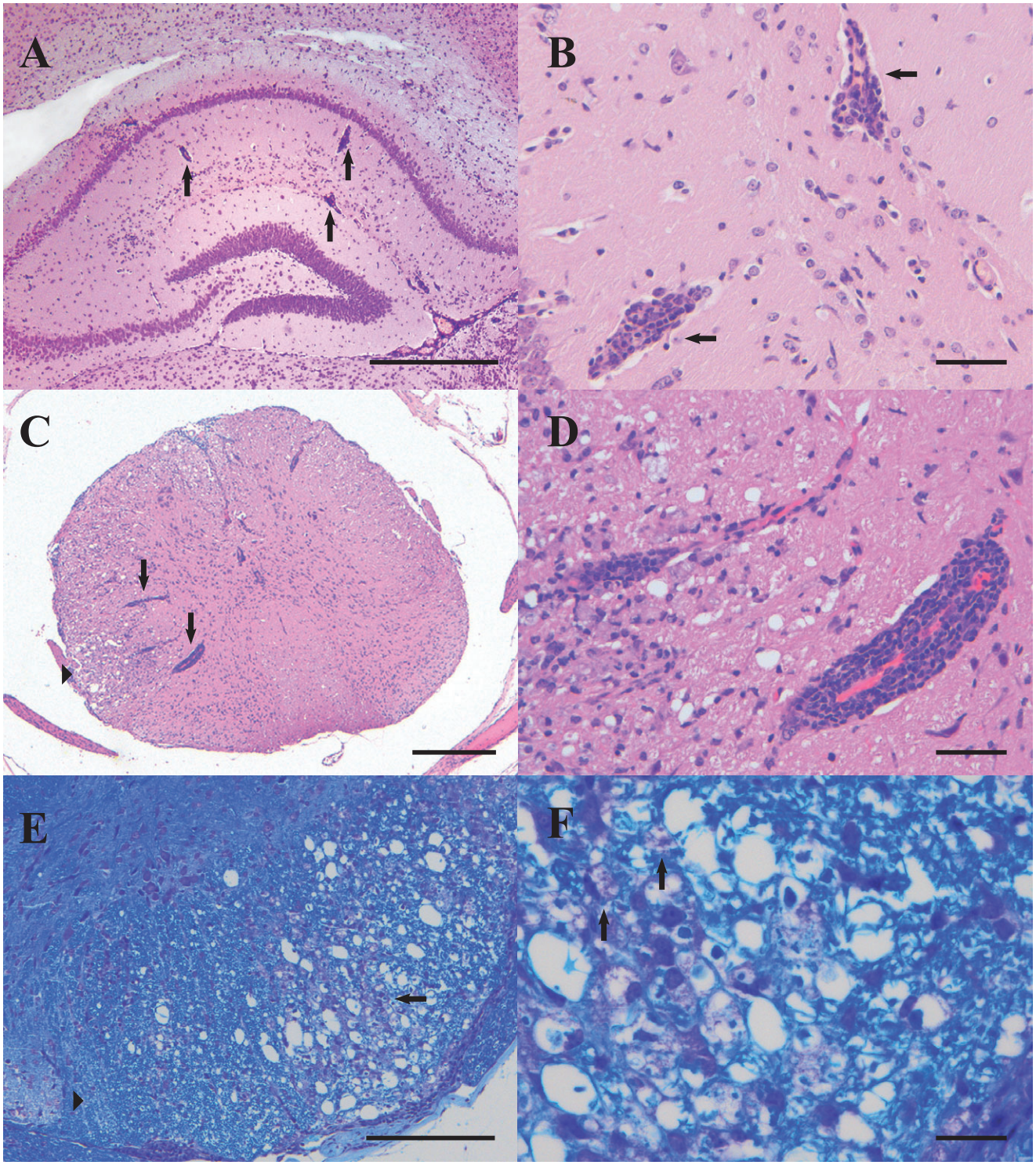

Figure 1. *Pathohistological changes in brain and spinal cord in Theiler's murine encephalomyelitis virus-infected mice.* (**A**) Transversal section of hippocampus displaying disseminated perivascular infiltration (arrows) at 14 days post infection (dpi). (**B**) Higher magnification from (**A**) displaying infiltration of immune cells in vessels (arrows). Hematoxylin and eosin. (**C**) Transversal section of the spinal cord displaying perivascular infiltration (arrows) and demyelination in the white matter (arrow head) at 98 dpi. (**D**) Higher magnification from (**C**) displaying infiltration of immune cells in vessels in the white matter. Hematoxylin and eosin. (**E**) Demyelinated area (arrow) and normal white matter (arrow head) in spinal cord at 196 dpi. (**F**) Higher magnification from (**E**) displaying macrophages/microglia with Gitter cell morphology (arrows) within the demyelinated white matter lesions. Luxol fast blue-cresyl violet. Scale bars = (**A**) 500 μm; (**B**) 50 μm; (**C**) 100 μm; (**D**) 25 μm; (**E**) 250 μm; (**F**) 50 μm.

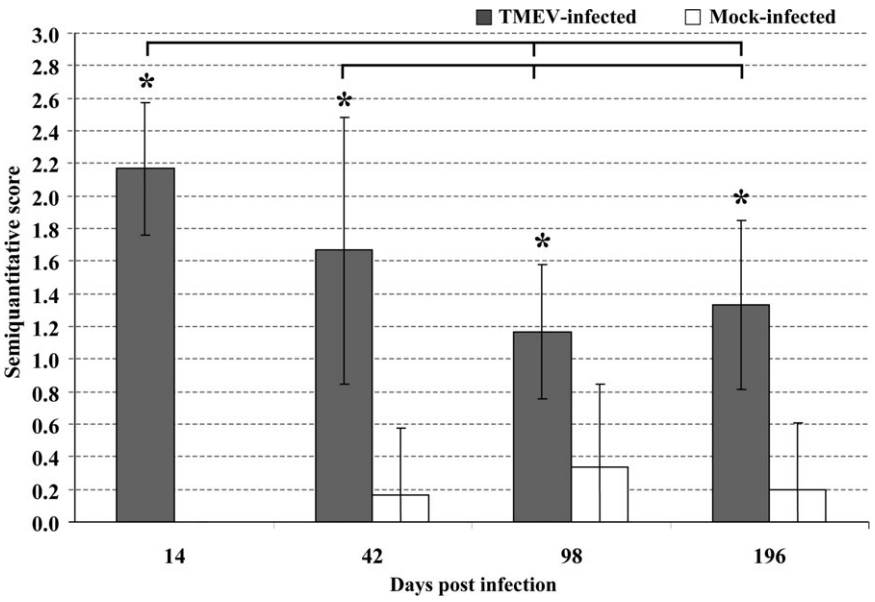

Figure 2. *Semiquantitative assessment of pathohistological changes in brain during Theiler's murine encephalomyelitis.* Increased perivascular infiltration is observed during the acute phase of the disease, progressively declining until 98 dpi, and moderately increasing during the late chronic phase in Theiler's murine encephalomyelitis virus-infected mice. Columns show the semi-quantitative score average and standard deviation. A significant difference between the groups, infected (n = 47) and sham-infected animals (n = 48), as detected by the Mann–Whitney *U*-tests is marked as follows: $*P < 0.05$. Significances between time points were analyzed with one-way ANOVA and Tukey *post-hoc* test; different bars denote statistically significant groups at a 0.05%.

at later time points (Figure 2). Inflammation was located predominantly in the cerebral grey matter (polioencephalitis) at 14 dpi, while at 42, 98 and 196 dpi inflammatory responses associated with myelin damage were largely restricted to the brainstem. Mann–Whitney *U*-test revealed significant differences among TMEV- and sham-infected mice over the study period.

Pathohistological examination of the spinal cord sections revealed a mononuclear inflammation within the white matter of TMEV-infected mice beginning at 14 dpi. The inflammatory changes increased toward 98 dpi (Figure 1C,D). The first demyelinated foci were observed at 42 dpi. The amount of demyelination progressively increased until 196 dpi (Figure 1E,F). Statistical comparisons employing Mann–Whitney *U*-test displayed a significantly higher degree of perivascular infiltration in the white matter from 14 to 196 dpi (Figure 3A), and of demyelination from 42 to 196 dpi in TMEV-infected compared with sham-infected mice (Figure 3B).

Viral detection by immunohistochemistry and *in situ* hybridization

Viral antigen and RNA were detected in TMEV-infected animals in association with inflammatory and demyelinating lesions of the brain and spinal cord. No virus was found in the deep cLN and spleen by immunohistochemistry and *in situ* hybridization, respectively, at early or late time points of the infection. In addition, virus was not present in the CNS, deep cLN or spleen of sham-infected mice.

Immunophenotyping of deep cLN

In comparison with sham-infected mice, significant increases of CD68- and lysozyme-positive cells in TMEV-infected mice (Figure 4) were found in the follicles of the deep cLN of TMEV-infected mice (CD68: $P = 0.0097$; lysozyme: $P = 0.0309$; Figure 5), while no significant differences were found in the lymph node paracortex or subcapsular sinus at this time point. In addition, statistical analysis revealed no phenotypical changes in the different anatomical areas of the deep cLN at later time points (42, 98 and 196 dpi).

Analysis of major transcriptional changes in TME

After running the EDGE natural cubic spline analysis for the 45101 probes of the GeneChip® mouse genome 430 2.0 arrays 425 probe sets in the deep cLN and 6 probe sets in the spleen were differentially expressed in TMEV-infected mice over the study period at a FDR of <5.0% (Q-value <0.05). Log_2 mean FCs of the individual time points of the differentially expressed genes in TMEV-infected versus sham-infected mice were calculated.

Results of the deep cLN showed that differentially expressed probe sets matched to 387 unique official gene symbols (Table S1). 27.4% of the genes (106/387 genes) presented FCs higher than ±1.5 at 14 dpi, while there were no gene transcriptions higher than ±1.5 FCs at later time points. In order to detect similarities in the expression patterns of the 387 differentially expressed genes of the lymph node, the log_2 mean FCs from sham-infected and TMEV-infected mice for each time point were analyzed through *k*-means cluster analyses and visualized through heat maps. The resulting five statistically significant *k*-mean clusters (*k*-means clusters I–V, Figure 6) grouped genes with similar expression. In order to assign a biological meaning to these genes, the functional annotation tool from DAVID was applied to all *k*-mean clusters, matching to a functional annotation cluster (Table S7). At this, *k*-means cluster I showed 156 genes (Table S2). One hundred percent of them were up-regulated at 14 dpi, while 13.5% were up-regulated at 42 dpi, 10.3% were up-regulated at 98 dpi and 71.2% of genes were up-regulated at 196 dpi. At 14 dpi, 7.7% of genes presented FCs higher than ±1.5. Genes grouped in this cluster were significantly associated (FDR < 1.0%) to gene ontology terms such as *mRNA processing*, *purine* and *pyrimidine nucleoside triphosphate metabolic processes* (Table S7).

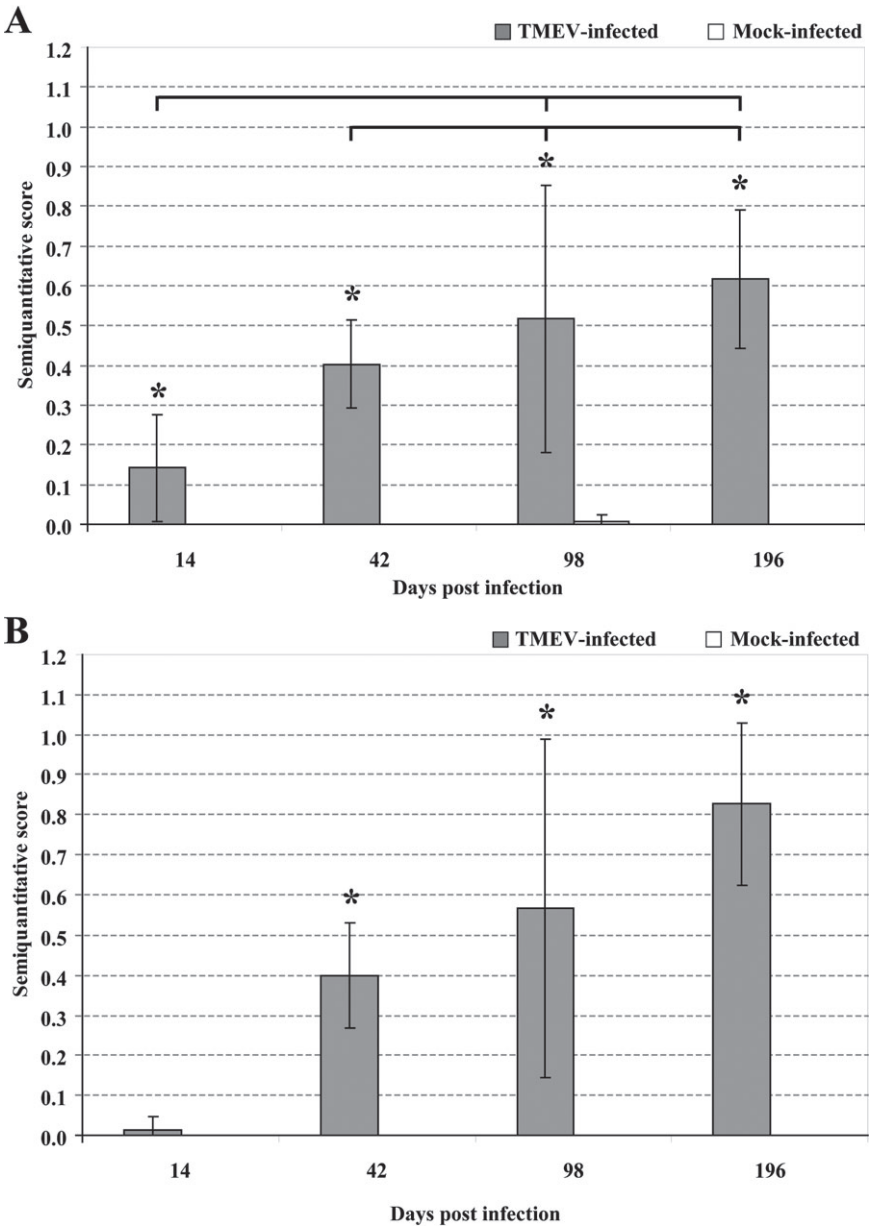

Figure 3. *Semiquantitative assessment of pathohistological changes in the spinal cord during Theiler's murine encephalomyelitis.* (**A**) Perivascular infiltrates in the white matter revealed significant differences between infected (n = 47) and sham-infected animals (n = 48) all through the study period, showing a progressive demyelination (**B**) in Theiler's murine encephalomyelitis virus-infected mice, starting at 42 dpi until the last time period. Columns show the semiquantitative score average and standard deviation. A significant difference between the groups as detected by the Mann–Whitney *U*-tests is marked as follows: **P* < 0.05. Significances between time points were analyzed with one-way ANOVA and Tukey *post-hoc* test; different bars denote statistically significant groups at a 0.05%.

K-means cluster II was composed of 89 genes (Table S3). 98.9% were down-regulated at 14 dpi, while 82.0% and 80.9% of genes showed an up-regulation at 42 and 98 dpi, respectively. A down-regulation of 56.2% of genes was observed at the last time point. The enriched gene ontology term for this cluster was significantly associated (FDR = 0.26%) to *protein metabolic processes* (Table S7).

K-means cluster III included 41 genes. All genes were up-regulated at 14 dpi with FCs >1.5 (Table S4), including the 10 most up-regulated genes throughout the study period (Table S8). All of these genes were down-regulated at 42 dpi, and 95.1% of them were down-regulated at 98 dpi. At 196 dpi, 97.6% of cluster III genes were up-regulated. According to DAVID, the most enriched ontology terms (FDR < 1.0%) for this cluster were *positive regulation of immune response*, *B-cell mediated immunity*, *regulation of immune response*, *complement activation* and *regulation of B-cell-mediated immunity* (Table S7).

K-means cluster IV grouped 73 genes in total (Table S5). All genes grouped within this cluster were down-regulated at 14 dpi, and 33.8% of them were presented with FCs >1.5. There was no enriched functional annotation cluster for this cluster from DAVID (Table S7), as the highest ranked ontology term did not meet the cutoff selection criteria of FDR < 1.0% (FDR = 6.0%). Therefore, a specific ontology term could not be assigned to cluster IV.

From the 28 genes reported in *k*-means cluster V (Table S6), 32.1% belong to the 10 most down-regulated genes at 14 dpi with a FC of <−1.5 (Table S9). Up-regulated genes in this cluster were observed at 42 and 98 dpi (89.3% and 92.9%, respectively). At the last time point (196 dpi), 64.3% of the genes were down-regulated.

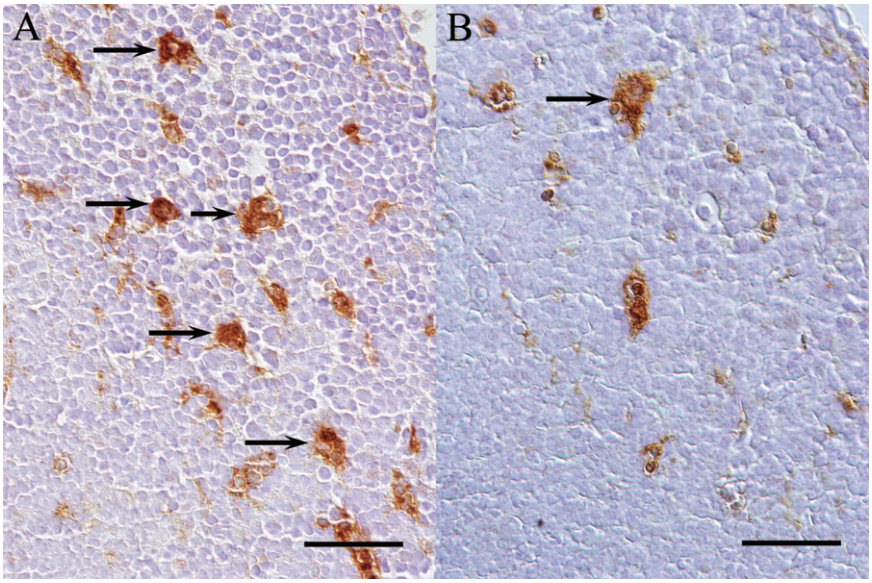

Figure 4. *Lysozyme-positive cells in the central nervous system-draining lymph node of Theiler's murine encephalomyelitis virus (TMEV)- and sham-infected mice.* (**A**) Increased numbers of lysozyme-positive cells (arrows) in the follicular area of the deep cervical lymph node of a TMEV-infected mouse at 14 days post infection. (**B**) Note the comparatively low number of lysozyme-positive cells (arrow) in the lymph node follicle of a sham-infected control animal at the same time point. Immunohistochemistry counterstained with Mayer's hemalaun. Scale bars = 50 µm.

The ontology term significantly related (FDR = 0.62%) to this cluster was *contractile fiber part pathway*.

In the spleen, differentially expressed probe sets matched to six unique official gene symbols related to cellular processes, such as cell division and metabolism (Table S10). However, genes could not be grouped using the *k*-mean clustering analysis.

DISCUSSION

In the present study, DNA microarray technology was used to identify transcriptional alterations in lymphoid organs of TMEV-infected SJL-mice. The most prominent changes in gene expression (up- or down-regulation) were found in the deep cLN during the acute disease phase at 14 dpi, followed by a decline of transcriptional changes at later time points. The silencing of gene transcription in the lymph node during the chronic phase at 42 and 98 dpi coincides with viral elimination in the cerebrum and TMEV persistence as well as demyelination in the brain stem and the spinal cord. Similarly, McMahon *et al* demonstrate that the CNS, and not the cLN or other peripheral lymphoid organs, is the major site of epitope spreading and activation of autoaggressive immune cells in EAE and TMEV during disease progression (54). In MS patients, the closure of the BBB, isolating the CNS from peripheral lymphoid organs, is supposed to play an important role in prolonged neuroinflammation and therapy failure (43, 53). This compartmentalization represents an inflammation process that became trapped behind the BBB, favoring local antigen presentation, plasma cells formation and antibody production within the brain in progressive MS lesions (29, 42, 43, 55, 66). However, so far, the onset and potential temporal changes of this phenomenon remain undetermined (55, 75).

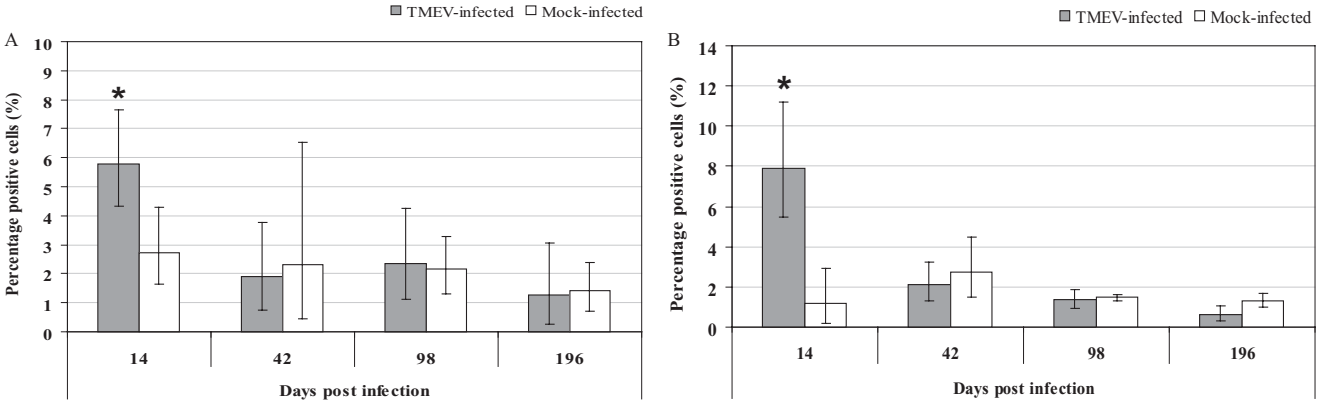

Figure 5. *Quantification of CD68- and lysozyme-positive cells in the follicle of the deep cervical lymph node of Theiler's murine encephalomyelitis virus (TMEV)- and sham-infected mice.* Immunohistochemistry revealed a significant increase of the percentage of CD68- (**A**) and lysozyme-positive cells (**B**) in TMEV-infected animals in comparison to sham-infected mice at 14 days post infection. Columns display average values and standard deviations. Significant difference ($P < 0.05$) between the groups as detected by two-way ANOVA with *post-hoc* test for multiple pairwise comparisons with Bonferroni adjustment is marked as follows: $*P < 0.05$.

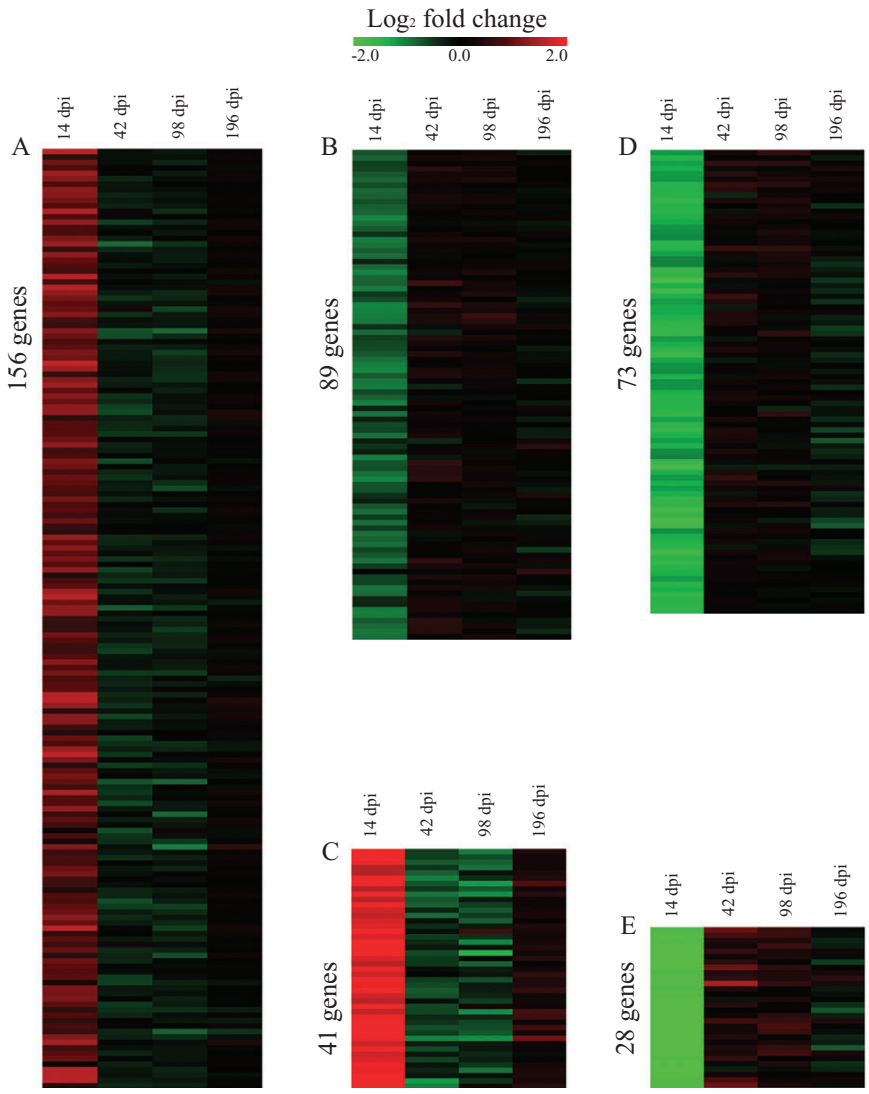

Figure 6. *Expression profile of differentially expressed genes in the deep cervical lymph node.* The fold changes of the 387 differentially genes were grouped by *k*-means cluster analysis to reveal similar expression patterns. Each row represents one of the 387 genes and each column one of four experimental days (14, 42, 98 and 196 days post infection). The log_2-transformed fold changes are indicated by a color scale ranging from –2 [relative low expression in Theiler's murine encephalomyelitis virus (TMEV)-infected mice] in green to 2 (relative high expression in TMEV-infected mice) in red. The majority of the differentially expressed genes were organized into five *k*-means cluster (I-V). (**A**) Represents *k*-means cluster I, showing gene up-regulation in the acute phase of TME. (**B**) *K*-means cluster II, consisted of down-regulated genes during the acute phase. (**C**) *K*-means cluster III, presented gene up-regulation at the acute phase. (**D**) and (**E**) are *k*-means cluster IV and V, respectively, presenting down-regulation of genes during the acute phase.

Results obtained in this study document the association between the B-cell response, antigen presenting cell activation and complement gene expression (*k*-means cluster III) in the deep cLN with TMEV-induced polioencephalitis at 14 dpi. These responses are supposed to be virus triggered (73) and might lead to immune cell activation associated with subsequent myelin damage in the spinal cord. Referring to this, the reactivation of the same gene cluster in the deep cLN at a late time point (196 dpi) may reflect the immune-mediated stage of the disease, accompanied by viral persistence and progressive spinal cord demyelination. Notably, previous DNA microarray analyses of the spinal cord of TMEV-infected mice (85) showed that the major transcriptional changes related to the immune response occur during disease progression. Accordingly, the minimal transcriptional changes detected at 42 and 98 dpi in the deep cLN node support the assumption of a closed BBB. Similarly to this finding, tracer studies revealed that the damage of the neurovascular endothelium is reduced in chronic lesions in EAE (35). In TME, leukocyte transmigration is regulated by adhesion molecules in the CNS, such as the intercellular adhesion molecule-1 (ICAM-1) and vascular cell adhesion molecule-1, as well as the expression of metalloproteinases by glial cells (37). Antiadhesion molecule therapy during the early disease phase reduces subsequent delayed type hypersensitivity and lesion progression in TMEV-infected mice (57, 79). However, as ICAM-1-deficient mice are not protected from TMEV-induced chronic demyelination, the exact role of the BBB remains to be determined (19). The present analyses suggest that the CNS is isolated between 42 and 98 dpi, but not completely compartmentalized at 196 dpi. This leakage, possibly associated with a reopening of the barrier, might facilitate peripheral immune responses and leukocyte migration during the late TME stage. In agreement with this, Leech *et al* (44) demonstrated endothelial abnormalities in progressive MS lesion, indicative of an incomplete repair of the BBB induced by the proinflammatory milieu within the CNS.

Further, the importance of B-cells in TMEV-induced demyelination has been stressed in previous microarray analysis, demonstrating gene expression related to humoral immune responses during lesion development (85). The results of the present study show an

up-regulation of genes functionally related to immune regulation, humoral immune responses, and complement activation (*k*-mean cluster III) in the deep cLN at 14 and 196 dpi, while at 42 and 98 dpi the majority of these genes are down-regulated. This cluster, grouping genes related to B-cell-mediated immunity, emphasizing the importance of B-cells (46) during the evolution of TME in SJL-mice. The most up-regulated gene during the first time period, TYRO protein tyrosine kinase binding protein (Tyrobp, also called DAP12) has an immune signaling mediator function, being involved in the activation of Natural Killer cells, granulocytes, monocyte/macrophages, DC and a Th_1-response (41). Additionally, reports indicated that Tyrobp expression is increased in microglial cells and brain macrophages during the acute phase of EAE (18) and that the induction of inflammation in EAE is a Tyrobp-dependent event, as demonstrated in knock-out experiments (4). Interestingly, Tyrobp serves as a mediator for DC migration from peripheral organs to lymph nodes (71). Moreover, the CD68 gene, up-regulated gene at 14 dpi, is involved in DC maturation (5) and facilitates the migration of antigen presenting cells from brain to lymphoid organs (13). In addition, CD68 allows homing of macrophages and has an important function in stimulating phagocytic activity of macrophages (15, 70). Other DC-related genes up-regulated predominantly at the early phase include CD209a, which mediates DC precursor migration from blood to tissues (22). CD68- and/or CD209a-DC have been found in plaques but also in the nonlesional gray matter of MS patients (13). As DCs are responsible for antigen presenting inside the lymph node, these transcriptional changes seems to be involved in initiating immune responses in the early phase of TME. Present results also revealed an up-regulation of the CD55 gene predominately at 14 dpi. CD55 is a regulatory membrane protein, involved in accelerating the C3/C5 convertases decay, protecting cells from complement-mediated damage (52). Together with its ligand CD97 on activated lymphocytes (27), CD55 plays an important role in the activation, adhesion and migration of cells during inflammation (90). Regarding this, CD55 is highly expressed on endothelial cells within the CNS in MS, facilitating the migration of immune cells through the BBB (90). In murine EAE, CD55 inhibits myelin-specific T-cells and limits the damage caused by Th_{17}-immune responses and IFN-g-mediated inflammation within the brain (51).

Transcriptional changes in the regional lymph node related to immune regulation were substantiated by immunohistochemical phenotyping. Increased numbers of CD68- and lysozyme-positive histiocytic cells in the follicle of the deep cLN represent a requisite for B cell activation during the early TME phase. In addition, the lack of TMEV in peripheral lymphoid organs as demonstrated by immunohistochemistry and *in situ* hybridization is indicative of an immune response induced by CNS-derived antigen presenting cells rather than a direct reaction caused by a virus spread in the lymph node. Antiviral antibodies are detectable within 1 week after experimental infection and high neutralizing antibody titers as well as myelin basic protein-specific autoantibodies are seen in persistent TMEV infection (72, 82). Interestingly, according to the idea of compartmentalized humoral immune responses, antibody titers are higher in the CNS than in the serum of TMEV-infected animals (49, 83).

The other four *k*-means clusters detected in the present study showed varied ontology terms relating to specific biological pathways. Although the exact role of these genes remains to be determined, transcriptional changes obviously coincide with the initiation of immune responses, possibly being involved in the regulation of gene expression and metabolic processes within the lymph node.

In the spleen, differentially expressed genes were not related to specific immune functions. Further, the low gene transcription rate of the spleen indicated that TMEV infection induces predominately an immune response in CNS-draining lymph nodes rather than a generalized immune response. Accordingly, it has been demonstrated that naïve lymphocytes enter the inflamed CNS and are activated by local antigen presenting cells in TME, bypassing the need for activation in peripheral lymphoid organs (54). In addition, previous gene array analyses by Ulrich *et al* (85) have demonstrated the occurrence of antigen processing and presentation locally within the inflamed spinal cord of TMEV-infected mice during disease progression. In comparison, microarray analysis of spleen samples in murine EAE revealed an up-regulation of genes related to inflammation and migration of immune cells to the CNS (33). The observed differences are possibly attributed to the peripheral induction of a myelin-specific immune response in EAE, while TME is caused by intracerebral infection.

The present study reveals that several genes are associated with the peripheral immune response in early TME. Further, equivalent to the hypothesis of a closed BBB in progressive MS, reduced transcription of genes at later time points is indicative of a compartmentalization during lesion development in infected animals. However, partial reactivation of immunity-related genes during the late chronic phase might represent a consequence of a leaky BBB or polyphasic process, respectively. Future experiments have to focus on the dynamics of neurovascular permeability and the interaction between CNS and the peripheral immune response during disease initiation and progression in this model for human MS.

ACKNOWLEDGMENTS

The authors are grateful to Julia Schirrmeier and Petra Grünig (Department of Pathology, University of Veterinary Medicine Hannover) for their excellent technical assistance. Furthermore, we thank Anuschka Unold and Thomas Feidl (Department of Nonclinical Drug Safety, Boehringer Ingelheim Pharma GmbH & Co KG Biberach an der Riss) for their exceptional technical support.

María José Navarrete-Talloni has received financial support from the FP6 Marie Curie—Early Stage Training Fellowship (MEST-CT-2005-021014).

This study was supported by the Deutsche Forschungsgemeinschaft (DFG, BA 815/10-1).

REFERENCES

1. Abbott NJ (2004) Evidence for bulk flow of brain interstitial fluid: significance for physiology and pathology. *Neurochem Int* **45**:545–552.
2. Arthur AT, Armati PJ, Bye C, Heard RN, Stewart GJ, Pollard JD, Booth DR (2008) Genes implicated in multiple sclerosis pathogenesis from consilience of genotyping and expression profiles in relapse and remission. *BMC Med Genet* **9**:17.
3. Ashburner M, Ball CA, Blake JA, Botstein D, Butler H, Cherry JM *et al* (2000) Gene Ontology: tool for the unification of biology. *Nat Genet* **25**:25–29.

4. Bakker ABH, Hoek RM, Cerwenka A, Blom B, Lucian L, McNeil T *et al* (2000) DAP12-deficient mice fail to develop autoimmunity due to impaired antigen priming. *Immunity* **13**:345–353.
5. Banchereau J, Briere F, Caux C, Davoust J, Lebecque S, Liu Y-J *et al* (2000) Immunobiology of dendritic cells. *Ann Rev Immunol* **18**:767–811.
6. Bernard CC, de Rosbo NK (1991) Immunopathological recognition of autoantigens in multiple sclerosis. *Acta Neurol (Napoli)* **13**:171–178.
7. Bolstad BM, Irizarry RA, Astrand M, Speed TP (2003) A comparison of normalization methods for high density oligonucleotide array data based on variance and bias. *Bioinformatics* **19**:185–193.
8. Bradbury MW, Cserr HF, Westrop RJ (1981) Drainage of cerebral interstitial fluid into deep cervical lymph of the rabbit. *Am J Physiol* **240**:329–336.
9. Brück W, Lucchinetti C, Lassmann H (2002) The pathology of primary progressive multiple sclerosis. *Mult Scler* **8**:93–97.
10. Compston A, Coles A (2008) Multiple sclerosis. *Lancet* **372**:1502–1517.
11. Consortium IMSG (2008) Refining genetic associations in multiple sclerosis. *Lancet Neurol* **7**:567–569.
12. Cserr HF, Knopf PM (1992) Cervical lymphatics, the blood-brain-barrier and the immunoreactivity of the brain—a new view. *Immunol Today* **13**:507–512.
13. Cudrici C, Ito T, Zafranskaia E, Niculescu F, Mullen KM, Vlaicu S *et al* (2007) Dendritic cells are abundant in non-lesional gray matter in multiple sclerosis. *Exp Mol Pathol* **83**:198–206.
14. Dalcanto MC, Melvold RW, Kim BS, Miller SD (1995) Two models of multiple sclerosis: experimental allergic encephalomyelitis (EAE) and Theiler's murine encephalomyelitis virus (TMEV) infection. A pathological and immunological comparison. *Microsc Res Tech* **32**:215–229.
15. Damoiseaux JG, Dopp EA, Calame W, Chao D, MacPherson GG, Dijkstra CD (1994) Rat macrophage lysosomal membrane antigen recognized by monoclonal antibody ED1. *Immunology* **83**: 140–147.
16. De Vos AF, van Meurs M, Brok HP, Boven LA, Hintzen RQ, van der Valk P *et al* (2002) Transfer of central nervous system autoantigens and presentation in secondary lymphoid organs. *J Immunol* **169**:5415–5423.
17. Dennis G, Sherman B, Hosack D, Yang J, Gao W, Lane H, Lempicki R (2003) DAVID: database for annotation, visualization, and integrated discovery. *Genome Biol* doi:10.1186/gb-2003-4-9-r60.
18. Divangahi M, Yang T, Kugathasan K, McCormick S, Takenaka S, Gaschler G *et al* (2007) Critical negative regulation of immunopathology by signaling intracellular infection. *J Immunol* **179**:4015–4026.
19. Drescher KM, Zoecklein LJ, Rodriguez M (2002) ICAM-1 is crucial for protection from TMEV-induced neuronal damage but not demyelination. *J Neurovirol* **8**:452–458.
20. Fabriek BO, Zwernmer JNP, Teunissen CE, Dijkstra CD, Polman CH, Laman JD, Castelijns JA (2005) *In vivo* detection of myelin proteins in cervical lymph nodes of MS patients using ultrasound-guided fine-needle aspiration cytology. *J Neuroimmunol* **161**:190–194.
21. Fujinami RS (2001) Viruses and autoimmune disease—two sides of the same coin? *Trends Microbiol* **9**:377–381.
22. Geijtenbeek TB, Torensma R, van Vliet SJ, van Duijnhoven GC, Adema GJ, van Kooyk Y, Figdor CG (2000) Identification of DC-SIGN, a novel dendritic cell-specific ICAM-3 receptor that supports primary immune responses. *Cell* **100**:575–585.
23. Gerhauser I, Alldinger S, Baumgartner W (2007) Ets-1 represents a pivotal transcription factor for viral clearance, inflammation, and demyelination in a mouse model of multiple sclerosis. *J Neuroimmunol* **188**:86–94.
24. Greter M, Heppner FL, Lemos MP, Odermatt BM, Goebels N, Laufer T *et al* (2005) Dendritic cells permit immune invasion of the CNS in an animal model of multiple sclerosis. *Nat Med* **11**:328–334.
25. Gröters S, Alldinger S, Baumgärtner W (2005) Up-regulation of mRNA for matrix-metalloproteinases-9 and -14 in advanced lesions of demyelinating distemper leukoencephalitis. *Acta Neuropathol* **110**:369–382.
26. Gurevich M, Tuller T, Rubinstein U, Or-Bach R, Achiron A (2009) Prediction of acute multiple sclerosis relapses by transcription levels of peripheral blood cells. *BMC Med Genomics* **2**:46.
27. Hamann J, Vogel B, vanSchijndel GMW, vanLier RAW (1996) The seven-span transmembrane receptor CD97 has a cellular ligand (CD55, DAF). *J Exp Med* **184**:1185–1189.
28. Hatterer E, Touret M, Belin MF, Honnorat J, Nataf S (2008) Cerebrospinal fluid dendritic cells infiltrate the brain parenchyma and target the cervical lymph nodes under neuroinflammatory conditions. *Plos ONE* doi:10.1371/journal.pone.0003321.
29. Hochmeister S, Grundtner R, Bauer J, Engelhardt B, Lyck R, Gordon G *et al* (2006) Dysferlin is a new marker for leaky brain blood vessels in multiple sclerosis. *J Neuropathol Exp Neurol* **65**:855–865.
30. Hou W, Kang HS, Kim BS (2009) Th17 cells enhance viral persistence and inhibit T cell cytotoxicity in a model of chronic virus infection. *J Exp Med* **206**:313–328.
31. Huang da W, Sherman BT, Lempicki RA (2009) Systematic and integrative analysis of large gene lists using DAVID bioinformatics resources. *Nat Protoc* **4**:44–57.
32. Ibrahim SM, Mix E, Bottcher T, Koczan D, Gold R, Rolfs A, Thiesen HJ (2001) Gene expression profiling of the nervous system in murine experimental autoimmune encephalomyelitis. *Brain* **124**:1927–1938.
33. Jelinsky SA, Miyashiro JS, Saraf KA, Tunkey C, Reddy P, Newcombe J *et al* (2005) Exploiting genotypic differences to identify genes important for EAE development. *J Neurol Sci* **239**:81–93.
34. Kida S, Pantazis A, Weller RO (1993) CSF drains directly from the subarachnoid space into nasal lymphatics in the rat—anatomy, histology and immunological significance. *Neuropathol App Neurobiol* **19**:480–488.
35. Kitz K, Lassmann H, Karcher D, Lowenthal A (1984) Blood-brain barrier in chronic relapsing experimental allergic encephalomyelitis: a correlative study between cerebrospinal fluid protein concentrations and tracer leakage in the central nervous system. *Acta Neuropathol* **63**:41–50.
36. Kummerfeld M, Meens J, Haas L, Baumgartner W, Beineke A (2009) Generation and characterization of a polyclonal antibody for the detection of Theilers murine encephalomyelitis virus by light and electron microscopy. *J Virol Methods* **160**:185–188.
37. Kumnok J, Ulrich R, Wewetzer K, Rohn K, Hansmann F, Baumgartner W, Alldinger S (2008) Differential transcription of matrix-metalloproteinase genes in primary mouse astrocytes and microglia infected with Theiler's murine encephalomyelitis virus. *J Neurovirol* **14**:205–217.
38. Kurtzke JF (1993) Epidemiologic evidence for multiple-sclerosis as an infection. *Clin Microbiol Rev* **6**:382–427.
39. Kurtzke JF (2005) Epidemiology and etiology of multiple sclerosis. *Phys Med Rehabil Clin N Am* **16**:327–349.
40. Lake J, Weller RO, Phillips MJ, Needham M (1999) Lymphocyte targeting of the brain in adoptive transfer cryolesion-EAE. *J Pathol* **187**:259–265.
41. Lanier LL, Bakker ABH (2000) The ITAM-bearing transmembrane adaptor DAP12 in lymphoid and myeloid cell function. *Immunol Today* **21**:611–614.
42. Lassmann H (2008) Mechanisms of inflammation induced tissue injury in multiple sclerosis. *J Neurol Sci* **274**:45–47.
43. Lassmann H, Brück W, Lucchinetti CF (2007) The immunopathology of multiple sclerosis: an overview. *Brain Pathol* **17**:210–218.

44. Leech S, Kirk J, Plumb J, McQuaid S (2007) Persistent endothelial abnormalities and blood–brain barrier leak in primary and secondary progressive multiple sclerosis. *Neuropath App Neurobiol* **33**:86–98.
45. Leek JT, Monsen E, Dabney AR, Storey JD (2006) EDGE: extraction and analysis of differential gene expression. *Bioinformatics* **22**:507–508.
46. Leslie M (2009) Immunology. Take-charge B cells create a buzz. *Science* **325**:144–145.
47. Liblau R, Fontaine B, Baron-Van Evercooren A, Wekerle H, Lassmann H (2001) Demyelinating diseases: from pathogenesis to repair strategies. *Trends Neurosci* **24**:134–135.
48. Lipton HL (1975) Theiler's virus infection in mice. Unusual biphasic disease process leading to demyelination. *Infect Immun* **11**:1147–1455.
49. Lipton HL, Gonzalez-Scarano F (1978) Central nervous system immunity in mice infected with theiler's virus. I. Local neutralizing antibody response. *J Infect Dis* **137**:145–151.
50. Liston A, Kohler RE, Townley S, Haylock-Jacobs S, Comerford I, Caon AC *et al* (2009) Inhibition of CCR6 function reduces the severity of experimental autoimmune encephalomyelitis via effects on the priming phase of the immune response. *J Immunol* **182**:3121–3130.
51. Liu JB, Lin F, Strainic MG, An FQ, Miller RH, Altuntas CZ *et al* (2008) IFN-gamma and IL-17 production in experimental autoimmune encephalomyelitis depends on local APC-T cell complement production. *J Immunol* **180**:5882–5889.
52. Lublin DM, Atkinson JP (1989) Decay-accelerating factor—biochemistry, molecular-biology and function. *Annu Rev Immunol* **7**:35–58.
53. Massacesi L (2002) Compartmentalization of the immune response in the central nervous system and natural history of multiple sclerosis. Implications for therapy. *Clin Neurol Neurosurg* **104**:177–181.
54. McMahon EJ, Bailey SL, Castenada CV, Waldner H, Miller SD (2005) Epitope spreading initiates in the CNS in two mouse models of multiple sclerosis. *Nat Med* **11**:335–339.
55. Meinl E, Krumbholz M, Derfuss T, Junker A, Hohlfeld R (2008) Compartmentalization of inflammation in the CNS: a major mechanism driving progressive multiple sclerosis. *J Neurol Sci* **274**:42–44.
56. Mendez-Fernandez YV, Hansen MJ, Rodriguez M, Pease LR (2005) Anatomical and cellular requirements for the activation and migration of virus-specific CD8(+) T cells to the brain during Theiler's virus infection. *J Virol* **79**:3063–3070.
57. Mestre L, Docagne F, Correa F, Loria F, Hernangomez M, Borrell J, Guaza C (2009) A cannabinoid agonist interferes with the progression of a chronic model of multiple sclerosis by down-regulating adhesion molecules. *Mol Cell Neurosci* **40**:258–266.
58. Miller SD, Olson JK, Croxford JL (2001) Multiple pathways to induction of virus-induced autoimmune demyelination: lessons from Theiler's virus infection. *J Autoimmun* **16**:219–227.
59. Mix E, Ibrahim S, Pahnke J, Koczan D, Sina C, Bottcher T *et al* (2004) Gene-expression profiling of the early stages of MOG-induced EAE proves EAE-resistance as an active process. *J Neuroimmunol* **151**:158–170.
60. Mix E, Pahnke J, Ibrahim SM (2002) Gene-expression profiling of experimental autoimmune encephalomyelitis. *Neurochem Res* **27**:1157–1163.
61. Monteyne P (1999) Multiple sclerosis: a secretive disease. *Biomed Pharmacother* **53**:341–343.
62. Monteyne P, Bureau JF, Brahic M (1997) The infection of mouse by Theiler's virus: from genetics to immunology. *Immunol Rev* **159**:163–176.
63. Njenga MK, Marques C, Rodriguez M (2004) The role of cellular immune response in Theiler's virus-induced central nervous system demyelination. *J Neuroimmunol* **147**:73–77.
64. Oleszak EL, Kuzmak J, Good RA, Platsoucas CD (1995) Immunology of Theiler's murine encephalomyelitis virus infection. *Immunol Res* **14**:13–33.
65. Ota K, Matsui M, Milford EL, Mackin GA, Weiner HL, Hafler DA (1990) T-cell recognition of an immunodominant myelin basic-protein epitope in multiple sclerosis. *Nature* **346**:183–187.
66. Owens GP, Bennett JL, Lassmann H, O'Connor KC, Ritchie AM, Shearer A *et al* (2009) Antibodies produced by clonally expanded plasma cells in multiple sclerosis cerebrospinal fluid. *Ann Neurol* **65**:639–649.
67. Panitch HS (1994) Influence of infection on exacerbations of multiple scelrosis. *Ann Neurol* **36**:S25–S28.
68. Pevear DC, Calenoff M, Rozhon E, Lipton HL (1987) Analysis of the complete nucleotide sequence of the Picornavirus Theiler's murine encephalomyelitis virus indicates that it is closely related to Cardiovirus. *J Virol* **61**:1507–1516.
69. Phillips MJ, Needham M, Weller RO (1997) Role of cervical lymph nodes in autoimmune encephalomyelitis in the Lewis rat. *J Pathol* **182**:457–464.
70. Ramprasad MP, Terpstra V, Kondratenko N, Quehenberger O, Steinberg D (1996) Cell surface expression of mouse macrosialin and human CD68 and their role as macrophage receptors for oxidized low density lipoprotein. *Proc Natl Acad Sci USA* **93**:14833–14838.
71. Randolph GJ, Sanchez-Schmitz G, Angeli V (2005) Factors and signals that govern the migration of dendritic cells via lymphatics: recent advances. *Springer Semin Immunopathol* **26**:273–287.
72. Rauch HC, Montgomery IN (1986) The role of the immune response in TMEV infection and the development of late onset demyelination. *J Immunol* **136**:2136–2140.
73. Rodriguez M, Lucchinetti CF, Clark RJ, Yaksh TL, Markowitz H, Lennon VA (1988) Immunoglobulins and complement in demyelination induced in mice by Theiler's virus. *J Immunol* **140**:800–806.
74. Saeed AI, Sharov V, White J, Li J, Liang W, Bhagabati N *et al* (2003) TM4: a free, open-source system for microarray data management and analysis. *Biotechniques* **34**:374–378.
75. Serafini B, Rosicarelli B, Magliozzi R, Stigliano E, Aloisi F (2004) Detection of ectopic B-cell follicles with germinal centers in the meninges of patients with secondary progressive multiple sclerosis. *Brain Pathol* **14**:164–174.
76. Sospedra M, Martin R (2005) Immunology of multiple sclerosis. *Ann Rev Immunol* **23**:683–747.
77. Soukas A, Cohen P, Socci ND, Friedman JM (2000) Leptin-specific patterns of gene expression in white adipose tissue. *Genes Dev* **14**:963–980.
78. Storey JD, Xiao WZ, Leek JT, Tompkins RG, Davis RW (2005) Significance analysis of time course microarray experiments. *Proc Natl Acad Sci USA* **102**:12837–12842.
79. Suidan GL, Dickerson JW, Chen Y, McDole JR, Tripathi P, Pirko I *et al* (2010) CD8 T cell-initiated vascular endothelial growth factor expression promotes central nervous system vascular permeability under neuroinflammatory conditions. *J Immunol* **184**:1031–1040.
80. Thompson AJ, Polman CH, Miller DH, McDonald WI, Brochet B, Filippi M *et al* (1997) Primary progressive multiple sclerosis. *Brain* **120**:1085–1096.
81. Tsunoda I (2008) Axonal degeneration as a self-destructive defense mechanism against neurotropic virus infection. *Future Virol* **3**:579–593.
82. Tsunoda I, Fujinami RS (1996) Two models for multiple sclerosis: experimental allergic encephalomyelitis and Theiler's murine encephalomyelitis virus. *J Neuropathol Exp Neurol* **55**:673–686.
83. Tsunoda I, Fujinami RS (2009) Neuropathogenesis of Theiler's Murine Encephalomyelitis Virus Infection, An Animal Model for

Multiple Sclerosis. *J Neuroimmune Pharmacol* [Epub ahead of print; doi: 10.1007/s11481-009-9179-x].
84. Ulrich R, Baumgartner W, Gerhauser I, Seeliger F, Haist V, Deschl U, Alldinger S (2006) MMP-12. MMP-3, and TIMP-1 are markedly up-regulated in chronic demyelinating theiler murine encephalomyelitis. *J Neuropathol Exp Neurol* **65**:783–793.
85. Ulrich R, Kalkuhl A, Deschl U, Baumgärtner W (2009) Machine learning approach identifies new pathways associated with demyelination in a viral model of multiple sclerosis. *J Cell Mol Med* [Epub ahead of print; doi: 10.1111/j.1582-4934.2008.00646.x].
86. Ure D, Rodriguez M (2005) Histopathology in the Theiler's virus model of demyelination. In: *Experimental Models of Multiple Sclerosis*, E Lavi, C Constantinescu (eds), pp. 579–591. Springer: New York.
87. Van Zwam M, Huizinga R, Heijmans N, van Meurs M, Wierenga-Wolf AF, Melief MJ *et al* (2008) Surgical excision of CNS-draining lymph nodes reduces relapse severity in chronic-relapsing experimental autoimmune encephalomyelitis. *J Pathol* **217**:543–551.
88. Van Zwam M, Huizinga R, Melief MJ, Wierenga-Wolf AF, van Meurs M, Voerman JS *et al* (2008) Brain antigens in functionally distinct antigen-presenting cell populations in cervical lymph nodes in MS and EAE. *J Mol Med* **87**:273–286.
89. Vega JL, Jonakait GM (2004) The cervical lymph nodes drain antigens administered into the spinal subarachnoid space of the rat. *Neuropathol Appl Neurobiol* **30**:416–418.
90. Visser L, de Vos AF, Hamann J, Melief MJ, van Meurs M, van Lier RAW *et al* (2002) Expression of the EGF-TM7 receptor CD97 and its ligand CD55 (DAF) in multiple sclerosis. *J Neuroimmunol* **132**:156–163.
91. Weller RO, Djuanda E, Yow HY, Carare RO (2009) Lymphatic drainage of the brain and the pathophysiology of neurological disease. *Acta Neuropathol* **117**:1–14.
92. Weller RO, Engelhardt B, Phillips MJ (1996) Lymphocyte targeting of the central nervous system: a review of afferent and efferent CNS-immune pathways. *Brain Pathol* **6**:275–288.

SUPPORTING INFORMATION

Additional Supporting Information may be found in the online version of this article:

Table S1. Official gene symbols, gene names and fold changes for all 387 gene probes sets differentially in the deep cervical lymph node at different time points.
Table S2. *K*-means cluster I. Official gene symbols, gene names and fold changes for all 156 gene probes sets differentially expressed in the deep cervical lymph node at different time points.
Table S3. *K*-means cluster II. Official gene symbols, gene names and fold changes for all 89 gene probes sets differentially expressed in the deep cervical lymph node at different time points.
Table S4. *K*-means cluster III. Official gene symbols, gene names and fold changes for all 41 gene probes sets differentially expressed in the deep cervical lymph node at different time points.
Table S5. *K*-means cluster IV. Official gene symbols, gene names and fold changes for all 73 gene probes sets differentially expressed in the deep cervical lymph node at different time points.
Table S6. *K*-means cluster V. Official gene symbols, gene names and fold changes for all 28 gene probes sets differentially expressed in the deep cervical lymph node at different time points.
Table S7. Significantly enriched pathways in the deep cervical lymph node.
Table S8. Official gene symbols, gene names and fold changes for the 10 most up-regulated genes in the deep cervical lymph node at different time points.
Table S9. Official gene symbols, gene names and fold changes for the 10 most down-regulated genes in the deep cervical lymph node at different time points.
Table S10. Official gene symbols, gene names and fold changes for all six gene probes sets differentially expressed in the spleen at different time points.

Please note: Wiley-Blackwell are not responsible for the content or functionality of any supporting materials supplied by the authors. Any queries (other than missing material) should be directed to the corresponding author for the article.